Cellular uptake of rigid elliptic random nanoparticles with a sensitivity evaluation

Sarah Iaquinta,[1] Shahram Khazaie,[1] Sylvain Fréour,[1] Frédéric Jacquemin,[1] Elena Ishow,[2] and Christophe Blanquart[3]

[1] *Institut de Recherche en Génie Civil et Mécanique (UMR CNRS 6183), Université de Nantes - Centrale Nantes, I.U.T. de Saint-Nazaire, Saint-Nazaire cedex, France**

[2] *Laboratoire Chimie Et Interdisciplinarité, Synthèse, Analyse, Modélisation (UMR CNRS 6230), University of Nantes, Nantes, France*

[3] *Center for Research in Cancerology and Immunology Nantes-Angers (UMR CNRS 6299, INSERM U892), University of Nantes, Nantes*

(Dated: June 23, 2021)

Abstract here

INTRODUCTION

The cellular uptake of nanoparticles (NP) has been studied as a potential cancer treatment for the past decades [1, 2]. Investigations have initially and mainly been conducted experimentally [3–8], while numerical studies have been emerging more recently [9–14], many of them focusing on the influence of the NP's shape.

In this work, we present a simplified model inspired from [15] – preferred over the more computationally expensive and more adapted to biochemical than mechanical approaches [16] molecular dynamics – of the cellular uptake of an elliptic NP to investigate the influence of the mechanical properties of the cell membrane and of the aspect ratio of the particle, after what a sensitivity analysis was conducted on these variables. To perform a purely mechanical approach, the study focuses on non specific endocytosis, in which adhesion is not due to ligand but to Van der Walls, electrostatic or hydrophobic interactions [16–18].

In order to take into consideration the real-world manufacturing challenges related to NP, it is necessary to identify the sensitivity of the uptake of NP to those parameters. Indeed, knowing this data allows the manufacturers to prioritize some properties over others, according to the ones that are easier for them to reliably produce [19].

The novelty of this work is to:

- clarify the model already exposed in the literature [15, 16, 20];
- present complementary results from the ones commonly exposed in literature;
- provide a biophysical explanation of them;
- provide a sensitivity analysis of the results to the different investigated parameters.

The document is organized as follows: section ref!presents the hypotheses, the model, and the investigation strategy adopted, with a broad description of the sensibility analysis performed (section) ref!. Next, section ref!provides an overview of the results obtained from the investigations, highlighting separately the influence of the cell membrane's mechanical properties and aspect ratio of the particle and the sensitivity of the endocytosis to these parameters. Following, section ref!provides a discussion of the results and hypotheses. Finally, section ref!wraps the results and discussions with the concluding remarks and perspectives for further work.

METHODS

Investigation strategy and hypotheses

In order to identify the influence of the mechanical properties of the cell membrane and of the aspect ratio $\bar{r}$ of the particle, the following strategy was adopted:

1. Identification of the influence of the mechanical properties of the cell membrane with a rigid circular NP;
2. Identification of the aspect ratio of a rigid elliptic particle for a range of a cell's mechanical properties;
3. Coupling of the influence of the aspect ratio of the rigid elliptic NP and of the cell's mechanical properties;
4. Building a metamodel;

5. Sensibility analysis of the former parameters on the cellular uptake of NPs.

This model focuses on the non-selective endocytosis of a rigid elliptic nanoparticle and does not apply to the specific cells of immunity (macrophages, phagocytes, etc...), as their physiology is specific to engulf objects from the extra-cellular middle [21].

In this paper, the investigations focus on rigid particles for two reasons: the first one is the calculation cost and complexity, the second one is to conduct a study with a reasonable amount of investigated variables. Nonetheless, given that the rigidity of the NP is typically at least 2 orders of magnitude greater than the one of the cell membrane [14, 19, 22], the assumption of a rigid NP is realistic in most cases.

The particle is supposed to be ≈ 10 smaller than the cell. Consequently, this study will focus on NP with perimeters around 200πnm, which matches with part of the NPs commonly used for drug delivery [14], while cell's diameter is in the order of the μm [23].

A 2D model of the system is used for the sake of simplification – and to save computation costs – and could have been performed in 3D without loss of generality [24].

In this paper, all the investigated parameters are supposed constant during endocytosis.

The model consists in evaluating the variation of total energy during the endocytosis and then identifying the wrapping degree at equilibrium.

Nanoparticle - membrane system

The system is illustrated in figure 1.

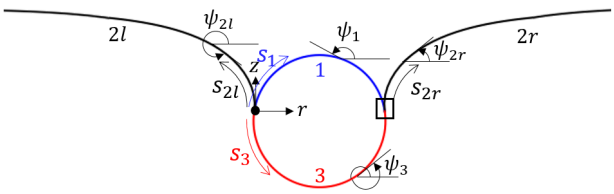

FIG. 1: Illustration of the nanoparticle-membrane interaction and the coordinates.

It is divided in 4 regions: region 1 is the free part of the particle, region $2r$ and $2l$ are the free parts of the membrane, respectively on the right and left sides of the particle and region 3 is the contact region between the particle and the membrane. The spatial coordinates are described with the tuple (r, z) wherein the origin is located at the intersection between the regions 1, $2l$ and 3. Each region is parametrized by its arclength s, between 0 and l, and by the angle ψ used to compute the curvature – necessary to evaluate the bending energy (equation 2). The system is symmetric, therefore the length of the two free parts of the membrane are equal ($l_{2l} = l_{2r}$) and will further be denoted as l_2.

The lengths l_1 and l_3 are defined in the terms of the wrapping degree f, which corresponds to the fraction of the particle already wrapped by the membrane. Hence, $l_3 = p \cdot f$, $l_1 = p(1-f)$ and $f = l_3(l_1 + l_3)^{-1}$, where p is the perimeter of the particle. The membrane is supposed to flatten the further it is from the nanoparticle, as its effects on the membrane weakens. The length on the free membrane l_2 depends linearly on the size of the NP, in order to be independent from the size of the NP. Indeed, two particles with same aspect ratio but different semi-major and semi-minor axes will give the same result. Consequently, all the length will be represented in a non-dimensional scale for the sake of simplification. A convergence study was then conducted on l_2 to verify that setting $l_2 = 20a$ – where a is the relative radius of the ellipsoid, defined as the ratio between the perimeter of the particle and 2π – as in [12] satisfies the hypothesis of membrane flatness at both extremities.

Evaluation of the variation of energy

The total of energy can be described by Canham-Helfrich Hamiltonian [15, 20]. The variation of energy is due to the bending of the membrane $\Delta\varepsilon_b$, the adhesion between the particle and the membrane $\Delta\varepsilon_{\tilde{\gamma}}$ and the membrane tension $\Delta\varepsilon_{\bar{\sigma}}$. Hence, the former reads:

$$\Delta\varepsilon = \Delta\varepsilon_b + \Delta\varepsilon_{\tilde{\gamma}} + \Delta\varepsilon_{\bar{\sigma}} \tag{1}$$

The bending energy of the membrane is decomposed as [20]:

$$\begin{aligned}\Delta\varepsilon_b = &\frac{1}{2}\kappa_{2r}\int_0^{l_2}(\dot{\psi}_{2r} - \widetilde{c}_{2r})^2 ds_{2r} \\ &+\frac{1}{2}\kappa_{2l}\int_0^{l_2}(\dot{\psi}_{2l} - \widetilde{c}_{2l})^2 ds_{2l} \\ &+\frac{1}{2}\kappa_3\int_0^{l_3}(\dot{\psi}_3 - \widetilde{c}_3)^2 ds_3\end{aligned} \tag{2}$$

Where $\dot{\psi}$ denotes the derivative of ψ with respect to s. Since the membrane is considered initially flat, its initial curvature $\widetilde{c}$ is zero, leading to

$\widetilde{c}_{2r} = \widetilde{c}_{2l} = \widetilde{c}_3 = 0$. Moreover, the two sides of the free membrane having same properties, $\kappa_{2r} = \kappa_{2l}$, denoted as κ_2. The particle being considered rigid, it does not deform. Consequently, the bending of the region 3 is only due to the deformations of the membrane. Thus, the bending rigidity of the zone 3 is equal to that of the zone 2, *i.e.*: $\kappa_3 = \kappa_2$. Furthermore, as defined in the figure 1, $\psi_{2l} = 2\pi - \psi_{2r}$. As such, equation 2 becomes:

$$\Delta\varepsilon_b = \underbrace{\kappa_2 \int_0^{l_2} \dot{\psi}_{2r}^2 ds_2}_{\Delta\varepsilon_{b2}} + \underbrace{\frac{1}{2}\kappa_2 \int_0^{l_3} \dot{\psi}_3^2 ds_3}_{\Delta\varepsilon_{b3}} \tag{3}$$

The bending energy on the free part of the membrane is computed based on the evolution of $\psi_{2r}(s_2)$ [25]:

$$\psi_{2r}(s_2) = 4\arctan\left(\tan\left(\frac{\psi_{2r}(0)}{4}\right)\exp\left(-\frac{s_2}{a}\sqrt{\frac{\bar{\sigma}}{2}}\right)\right) \tag{4}$$

The spatial coordinates (r, z) in regions $2r$ and $2l$ are then evaluated as follows [26]:

$$r_{2r}(s_2) = r_{2r}(0) + s_2 - \sqrt{\frac{\bar{\sigma}}{2}}\frac{1-\cos\left(\psi_{2r}(0)\right)}{\coth\left(\sqrt{\frac{\bar{\sigma}}{2}}s_2\right) + \cos\left(\frac{\psi_{2r}(0)}{2}\right)} \tag{5a}$$

$$r_{2l}(s_2) = r_{2r}(0) - r_{2r}(s_2) \tag{5b}$$

$$z_{2r}(s_2) = z_{2r}(0) + \sqrt{\frac{8}{\bar{\sigma}}}\sin\left(\frac{\psi_{2r}(0)}{2}\right)\left[1 - \frac{\operatorname{csch}\left(\sqrt{\frac{\bar{\sigma}}{2}}s_2\right)}{\coth\left(\sqrt{\frac{\bar{\sigma}}{2}}s_2\right) + \cos\left(\frac{\psi_{2r}(0)}{2}\right)}\right] \tag{6a}$$

$$z_{2l}(s_2) = z_{2r}(s_2) \tag{6b}$$

In which $\psi_2(0)$ is the value of ψ_2 at the intersection between the regions 3 and $2r$ (represented with a square in the figure 1). The points $(s_{2r} = 0)$ and $(s_3 = l_3)$ are coincident. Consequently, $\psi_{2r}(s_2 = 0)$ can be calculated from $\psi_3(s_3 = l_3)$ which is well known from the definition of the ellipse (as well as ψ_1, r_1, z_1, r_3 and z_3). $\Delta\varepsilon_{b2}$ can then easily be computed.

The adhesion energy is defined as:

$$\Delta\varepsilon_\gamma = -\gamma l_3 \tag{7}$$

In which γ is the lineic adhesion force between the membrane and the particle.

The tension energy is defined as follows:

$$\Delta\varepsilon_\sigma = \sigma\Delta l \tag{8}$$

In which σ is the membrane tension and Δl is the length of stretched membrane.

Finally, in order to ease further comparison, the adimensional energy variation ΔE is introduced as $\Delta E = \Delta\varepsilon\frac{2a}{\kappa_2}$ and Eq. 1 is reformulated as Eq. 9, in which adimensional variables $\bar{\gamma}$ and $\bar{\sigma}$ are introduced as $\bar{\gamma} = \gamma\frac{2a^2}{\kappa_2}$ and $\bar{\sigma} = \sigma\frac{2a^2}{\kappa_2}$.

Measurements *in vivo* determined $\kappa_2 \approx 10^{-18}$N.m, $\gamma \approx 10^{-3}$N.m^{-1} and $\sigma \approx 10^{-5}$N.m^{-1} [16, 20, 27]. The units commonly used for these variables are k_BT or erg for κ_2, $k_BT.nm^{-2}$ or erg.cm^{-2} for γ and dyne.cm^{-1} for σ [16, 28, 29] but we chose to convert them in the U.S.I to allow an understanding by a larger audience.

$$\Delta E = \underbrace{\overbrace{\frac{a}{4}\int_0^{l_3}\dot{\psi}_3^2 ds_3}^{\Delta E_{b2}} + \overbrace{\frac{a}{4}\int_0^{l_2}\dot{\psi}_{2r}^2 ds_2}^{\Delta E_{b3}}}_{\Delta E_b} \underbrace{-\frac{1}{4a}\bar{\gamma}l_3}_{\Delta E_{\bar{\gamma}}} + \underbrace{\frac{1}{4a}\bar{\sigma}\left(2l_2 + l_3 - r_{2r}(l_2) + r_{2l}(l_2)\right)}_{\Delta E_{\bar{\sigma}}} \tag{9}$$

The evolution of ΔE with respect to f in the case of a circular NP is illustrated in the figure 4. The contributions of ΔE_b, $\Delta E_{\bar{\gamma}}$, $\Delta E_{\bar{\sigma}}$ on the total energy variation ΔE are presented in the figure 2.

Phases

The next step of the study consists in evaluating the influence of the aspect ratio $\bar{r}$ (ratio between the semi-major and semi-minor axes) of the particle on the wrapping degree at equilibrium, denoted f_{eq}. Contrary to circular NP, $\Delta E(f)$ may have multiple local minima. It is then necessary provide a clear definition of equilibrium. According to the literature [26, 30], there is no mechanism that could contribute to overcome the barriers of energy following a local minimum, except the energy due to thermal fluctuation. However, thermal fluctuations are too weak to overcome the energy barriers we met in this study.

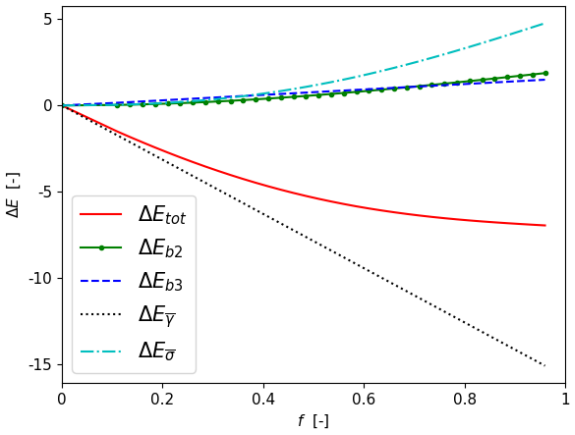

FIG. 2: Contribution of bending, adhesion and tension on the total energy variation, $\bar{\gamma} = 10$, $\bar{\sigma} = 2$.

Consequently, the equilibrium is defined as the first local minimum.

Three phases are defined (see figure 3). The first phase gathers the configurations which led to $f_eq < 0.2$. For this range of wrapping degree, one can consider that the endocytosis aborted soon after the particle touched the cell. There is *no wrapping*. The phase 3 gathers the configurations which led to an equilibrium where the two sides of free membrane crossed ($\max r_{2l}(s_{2l}) \geq \min r_{2r}(s_{2r})$). This is *full wrapping*, since the particle is already engulfed by the cell. The phase 2 is composed of all the remaining configurations, which led to *partial wrapping*.

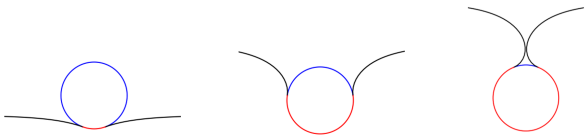

FIG. 3: Illustration of the 3 wrapping phases: no wrapping (left), partial wrapping (middle) and full wrapping (right).

To investigate the influence of the membrane tension $\bar{\sigma}$ and adhesion $\bar{\gamma}$, $\Delta E(f)$ is computed $\forall f \in [0, 1]$ for a given aspect ratio $\bar{r}$, say 1 (a circular NP), and a range of values of $\bar{\sigma}$ and $\bar{\gamma}$. It is necessary to set ranges of values because of the variability of these parameters (considering the variety of cell types and the heterogeneity of membrane composition [31, 32]). Based on the literature [12, 15, 24, 27] and considering a radius of 100 nm, the ranges were defined as $\bar{\sigma} \in [0.5, 5.5]$ and $\bar{\gamma} \in [1, 10]$. For each one of these testcases, the phase are identified, as illustrated in the figure 5.

From the phase diagram, one evaluates the proportion of each phase. Then, to investigate the influence of another parameter – here, the aspect ratio $\bar{r}$ of the elliptic particle – one generates the phase diagram and then the proportion of the three phases for each value of the investigated parameter and compare them in a phase comparison graph, as illustrated in the figure 10.

To investigate the influence of $\bar{r}$, the perimeter of the NP was fixed to 2π and the values of the semi-minor and semi-major axes were defined based on the approximation of the perimeter of an ellipse established by Ramanujan [33], for a given aspect ratio input value. The geometric parameters used to perform the investigation are detailed in the table I.

The results are presented in the section ref!.

SURROGATE MODELING AND SENSITIVITY ANALYSIS OF THE RANDOM WRAPPING ANGLE

The uncertainty quantification methods that will be subsequently used in this paper are briefly introduced in this section. Consider the positive, second-order stochastic wrapping degree F indexed on $\mathbb{R}^+$ as a function of a vector of M input random variables $\boldsymbol{X} = \{X_1, X_2, ..., X_M\}^\top \in \mathbb{R}^M$, i.e. $F = \Xi(\boldsymbol{X})$. To investigate the probabilistic content of the random variable F, the classical sampling techniques such as Monte Carlo (MC) simulation can be used. However, the convergence is guaranteed for large number of samples implying high computational costs that makes the method intractable. As such, metamodeling approach is an appropriate alternative allowing us to build fast-to-evaluate surrogate models using a limited number of calls to the numerical solver. For this purpose, we will use two popular surrogate models: Kriging [34–37] and Polynomial Chaos Expansion (PCE) [38–41] which are briefly discussed in Sections ref!and ref!. Finally in Section ref!, based on these surrogate modeling methods, the Sobol' indices are introduced to quantify the global sensitivities of F with respect to each input random variable.

Kriging

Kriging, also known as Gaussian process regression, is based on the decomposition of the random variable F into a deterministic mean (trend) and a residual Gaussian process as $\Xi^K(\boldsymbol{x}) = \boldsymbol{a}^\top \boldsymbol{g}(\boldsymbol{x}) +$

TABLE I: Geometric parameters of the investigated ellipses, the perimeter is set to 2π.

	vertical ellipse				circle	horizontal ellipse			
aspect ratio $\bar{r}$	1/6	1/4	1/3	1/2	1	2	3	4	6
semi-major axis	0.25	0.37	0.47	0.65	1	1.30	1.41	1.46	1.5
semi-minor axis	1.5	1.46	1.41	1.30	1	0.65	0.47	0.37	0.25

$\sigma^2 Z(\boldsymbol{x};\boldsymbol{\ell})$ [36]. In this equation $\boldsymbol{x}$ is a realization of the random vector $\boldsymbol{X}$, $\mathbb{E}[\Xi^K] = \boldsymbol{a}^\top \boldsymbol{g}(\boldsymbol{x})$ is the mean of F, represented by a coefficients vector $\boldsymbol{a}$ and a set of predefined shape functions $g_i, i \in \{0, ..., P-1\}$, and $Z(\boldsymbol{x};\boldsymbol{\ell})$ is a standard Gaussian random field. Note also that σ^2 represents the variance of the Kriging's residual and $^\top$ denotes the transposition. The stochastic part $Z(\boldsymbol{x};\boldsymbol{\ell})$ is defined by its auto-correlation function (ACF) $R(\boldsymbol{x}, \boldsymbol{x}';\boldsymbol{\ell}) = \mathbb{E}[Z(\boldsymbol{x};\boldsymbol{\ell})Z(\boldsymbol{x}';\boldsymbol{\ell})]$. The vector $\boldsymbol{\ell} = \{\ell_1, ..., \ell_M\}^\top$ is called the correlation distance and should be calculated.

The objective is to evaluate the unknown parameters using a sample of size N (aka experimental design), $\mathbf{X} = \{\boldsymbol{x_1}, ..., \boldsymbol{x_N}\}$ and the corresponding wrapping degrees $\mathbf{F} = \{f_1, ..., f_N\}^\top$ in which $f_i = \Xi(\boldsymbol{x_i})$, $i \in \{1, ..., N\}$ is the value of f for i^{th} realization of input parameters. The least-squares estimate of the $P \times 1$ coefficients vector $\boldsymbol{a}$ is $\hat{\boldsymbol{a}} = (\boldsymbol{G}^\top \boldsymbol{R}^{-1} \boldsymbol{G})^{-1} \boldsymbol{G}^\top \boldsymbol{R}^{-1} \mathbf{F}$ in which the $N \times P$ matrix $\boldsymbol{G}$ is defined as $G_{ij} = g_j(\boldsymbol{x_i})$, $i \in \{1, ..., N\}$, $j \in \{1, ..., P\}$ and $\boldsymbol{R}$ is the $N \times N$ correlation matrix whose components are $R_{ij} = R(|\boldsymbol{x}_i - \boldsymbol{x}_j|;\boldsymbol{\ell}), i, j \in \{1, ..., N\}$. The Kriging predictor at any point (realization of input parameters) $\boldsymbol{x}$ is a Gaussian random variable $\hat{F}(\boldsymbol{x}) \sim \mathcal{N}(\mu_{\hat{F}}(\boldsymbol{x}), \sigma_{\hat{F}}(\boldsymbol{x}))$ whose parameters could be obtained as follows (see [36] for more details):

$$\mu_{\hat{F}}(\boldsymbol{x}) = \boldsymbol{g}(\boldsymbol{x})^\top \hat{\boldsymbol{a}} + \boldsymbol{r}(\boldsymbol{x})^\top \boldsymbol{R}^{-1} (\mathbf{F} - \boldsymbol{G}\hat{\boldsymbol{a}}), \tag{10}$$

$$\sigma^2_{\hat{F}}(\boldsymbol{x}) = \sigma^2 \left(1 - \boldsymbol{r}(\boldsymbol{x})^\top \boldsymbol{R}^{-1} \boldsymbol{r}(\boldsymbol{x}) + \boldsymbol{u}(\boldsymbol{x})^\top (\boldsymbol{G}^\top \boldsymbol{R}^{-1} \boldsymbol{G})^{-1} \boldsymbol{u}(\boldsymbol{x}))\right), \tag{11}$$

in which $N \times 1$ vector $\boldsymbol{r}(\boldsymbol{x})$ specifies the correlation between each realization point $\boldsymbol{x}_i$ and the prediction point $\boldsymbol{x}$, *i.e.* $\boldsymbol{r}_i(\boldsymbol{x}) = R(|\boldsymbol{x} - \boldsymbol{x}_i|;\boldsymbol{\ell}), i \in \{1, ..., N\}$ and the $P \times 1$ vector $\boldsymbol{u}(\boldsymbol{x})$ is defined as $\boldsymbol{u}(\boldsymbol{x}) = \boldsymbol{G}^\top \boldsymbol{R}^{-1} \boldsymbol{r}(\boldsymbol{x}) - \boldsymbol{g}(\boldsymbol{x})$. Note also that the mean Kriging estimator interpolates the data, *i.e.* $\mu_{\hat{F}}(\boldsymbol{x}_i) = \Xi(\boldsymbol{x}_i)$ and $\sigma^2_{\hat{F}}(\boldsymbol{x}_i) = 0$, $i \in \{1, ..., N\}$. The main steps of the Kriging method are summarized bellow.

The first step consists in choosing the trend function. Then a model for the ACF R is chosen with a correlation length vector $\boldsymbol{\ell}$ to be determined. Then, using the experimental design $\boldsymbol{\mathcal{X}}$ and the values of the wrapping degree f_i, an optimization problem is solved for the vector $\boldsymbol{\ell}$. Maximum likelihood and cross-validation methods are frequently for this purpose [42, 43]. We use the maximum likelihood method which is based on the following optimization problem [44]:

$$\boldsymbol{\ell} = \arg \min_{\mathcal{D}_\theta = \mathbb{R}^{+M}} \left(\frac{1}{2} \log(\det(\boldsymbol{R})) + \frac{N}{2} \log(2\pi\sigma^2) + \frac{N}{2} \right). \tag{12}$$

Finally, the optimal values of $\boldsymbol{\ell}$ are used to obtain the coefficients of the trend $\hat{\boldsymbol{a}}$, the mean $\mu_{\hat{Y}}(\boldsymbol{x})$ and the variance $\sigma^2_{\hat{Y}}(\boldsymbol{x})$ of the Kriging predictor.

A leave-one-out (LOO) cross-validation error estimator ϵ_{LOO} is frequently used to assess the quality of the meta-models and/or to chose the best meta-model among several candidates. It is based on the creation of N surrogate models each of which lacks one point of the experimental design, *i.e.* $\boldsymbol{\mathcal{X}}^{(-j)} = \{\boldsymbol{x_i}, i = 1, ..., N, i \neq j\}$. One should then compare the corresponding predictions with the real value of the QoI at the excluded point [45]. **(author?)** [46] derived an analytical solution for ϵ^K_{LOO} without computing the N meta-models.

Polynomial Chaos Expansion (PCE)

PCE is a functional representation of the random QoI [47, 48] wherein the latter is written as an infinite linear combination of some orthogonal polynomials with respect to the PDFs of input parameters [49]. The exact infinite expansion is often truncated up to a certain degree p as:

$$\Xi^{PCE}_p(\boldsymbol{x}) = \sum_{i=0}^{P-1} a_i \Psi_i(\boldsymbol{\zeta}) = \boldsymbol{a}^\top \boldsymbol{\Psi}(\boldsymbol{\zeta}), \tag{13}$$

in which $P = \binom{p+M}{p}$ polynomials and deterministic coefficients are denoted with column vectors $\boldsymbol{\Psi}$ and $\boldsymbol{a}$, respectively. An isoprobabilistic transformation $\mathcal{T}$ links the standard random vector $\boldsymbol{\zeta} = (\zeta_1, ..., \zeta_M)$ to the random input vector $\boldsymbol{X}$, i.e. $\boldsymbol{X} = \mathcal{T}(\boldsymbol{\zeta})$.

The type of polynomials is determined based on the PDFs of the input random parameters. For instance, Legendre and Jacobi polynomials are used for uniform and beta random variables. The basis functions are then constructed by multiplying the one dimensional bases. The expansion coefficients calculated using a non-intrusive least squares approach via $\hat{\boldsymbol{a}} = (\boldsymbol{G}^\top \boldsymbol{G})^{-1}\boldsymbol{G}^\top \mathbf{F}$ wherein the $N \times P$ matrix $\boldsymbol{G}$ is defined as $G_{ij} = \Psi_j(\boldsymbol{\zeta}_i)$. The mean and variance of the random wrapping degree are subsequently calculated via $\mathbb{E}[\Xi_p^{PCE}] = a_0$ and $\mathrm{Var}[\Xi_p^{PCE}] = \sum_{i=1}^{P-1} a_i^2$, respectively. Finally, the Sobol' sensitivity indices are calculated as will be discussed in the next Section.

Sensitivity analysis

To calculate the sensitivity indices [50], we use Quasi Monte Carlo estimators for Kriging and direct estimations based on the expansion coefficients for PCE (see [51] for more details). A QMC-based estimator for the Sobol index of the random variable X_i $(1 \leq i \leq M)$ writes:

$$S_i = \frac{\sigma_i^2}{\sigma_{\hat{F}}^2} \simeq \frac{1}{N\sigma_{\hat{F}}^2} \sum_{j=1}^{N} \hat{F}_j(S_2)\left(\hat{F}_j(S_1^i) - \hat{F}_j(S_1)\right), \tag{14}$$

in which S_1 and S_2 are two independent QMC samples of size $N \times M$ of input random parameters and S_1^i is the matrix S_1 whose i-th column is replaced by the i-th column of S_2. Note that in (14) $\sigma_{\hat{F}}^2 = \mathrm{Var}[\hat{F}]$ is the estimate of the total variance of the random wrapping degree F and $\sigma_i^2 = \mathrm{Var}[\mathbb{E}[\hat{F}|X_i]]$ is the partial variance with respect to the random variable X_i or the share of variance of $\hat{F}$ resulting from X_i. The sensitivity of the wrapping degree to the interactions between input random variables X_i and X_j is described by the second order index S_{ij} $(1 \leq i \neq j \leq M)$ in which the marginal effects are not considered:

$$S_{ij} = \frac{\sigma_{ij}^2}{\sigma_{\hat{F}}^2} = \frac{\mathrm{Var}[\mathbb{E}[\hat{F}|X_iX_j]]}{\mathrm{Var}[\hat{F}]} - S_i - S_j, \tag{15}$$

which could be similarly generalized to higher order interactions. There are $2^M - 1$ Sobol indices that can be defined in which M is the stochastic dimension of the problem. In this paper we have $M = 3$ that yields $2^3 - 1 = 7$ different Sobol indices for different levels of interactions. Following **(author?)** [52], instead of calculating different indices for different order of interactions, total Sobol indices are used to estimate the total contribution of each random variable X_i $(1 \leq i \leq M)$ to the variance of the wrapping degree:

$$S_{T_i} = S_i + \sum_{i \neq j} S_{ij} + \sum_{(j<k) \neq i} S_{ijk} + ... \tag{16}$$

A QMC-based estimator for the total Sobol index reads:

$$S_{T_i} \simeq \frac{1}{2N\sigma_{\hat{F}}^2} \sum_{j=1}^{N} \left(\hat{F}_j(\Xi_1^i) - \hat{F}_j(\Xi_1)\right)^2. \tag{17}$$

As mentioned earlier, for PCE, the sensitivity indices could be analytically estimated in terms of the coefficients of the expansion. The readers are referred to **(author?)** [41] for more details.

RESULTS

Mechanical parameters $\bar{\gamma}$ and $\bar{\sigma}$

The mechanical parameters $\bar{\gamma}$ and $\bar{\sigma}$ tend to alter the evolution of ΔE with respect to f, as illustrated in the figure 4. Indeed, increasing $\bar{\gamma}$ tends to lower ΔE while increasing $\bar{\sigma}$ increases it. The membrane tension does not influence ΔE for $f < 0.2$, while the effect of $\bar{\gamma}$ is significant $\forall f$. This matches with the decomposition of ΔE presented in figure 2 in which one can see that ΔE_b and $\Delta E_{\bar{\sigma}}$ – the energy variations in which $\bar{\sigma}$ contributes – do not change for low f, contrary to $\Delta E_{\bar{\gamma}}$ which decreases significantly.

The conclusions from figure 4 apply to the range of values of $\bar{\gamma}$ and $\bar{\sigma}$ tested. Indeed, the phase diagram (figure 5) highlights that a large $\bar{gamma}$ and low $\bar{\sigma}$ are necessary to reach phase 3. That means that a NP is more likely to be uptaken by a cell whose membrane tension is low and which adheres well to the NP. These results match experimental studies and theoretical investigations [7, 8, 15, 53].

An illustration of the effect of membrane tension and adhesion on the wrapping is given in the figure 6. In this figure, even though the adhesion does not affect the shape of endocytosis, it is clear that for low membrane tension, the two sides of the membrane tend to get in contact more easily, which configures the full wrapping.

Aspect ratio of the elliptic particle

The aspect ratio $\bar{r}$ of the elliptic particle affects the evolution of ΔE with respect to f, as illustrated in the figure 7.

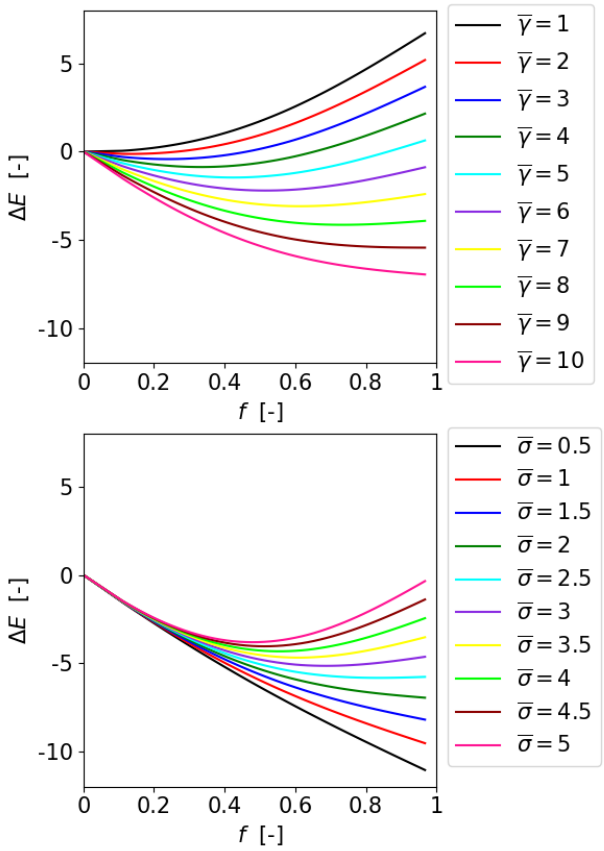

FIG. 4: Effect of adhesion (top) $\bar{\gamma}$ with $\bar{\sigma}=2$ and (bottom) membrane tension $\bar{\sigma}$ with $\bar{\gamma}=10$ on $\Delta E(f)$.

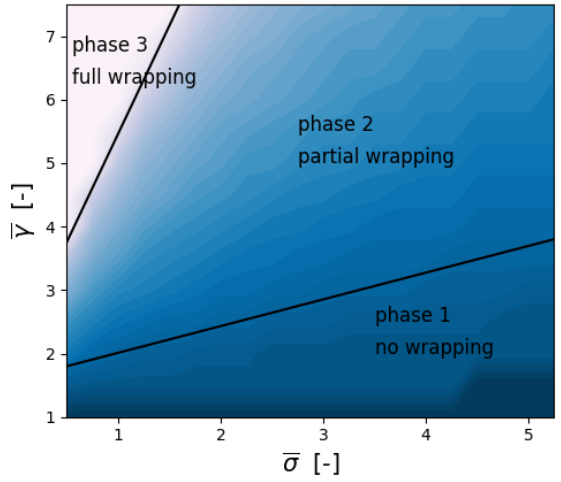

FIG. 5: Phase diagram for a circular NP. Colors: values of f_{eq}, from 0 (darkest) to 1 (lightest).

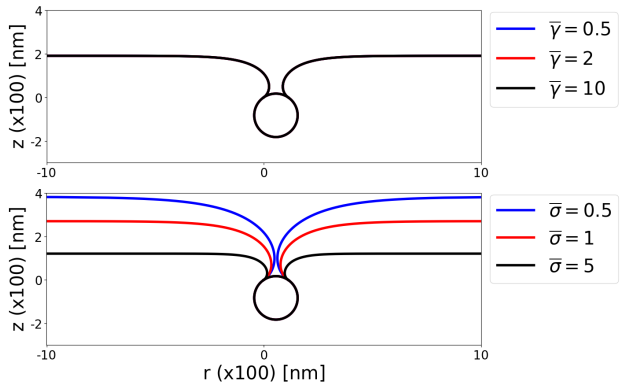

FIG. 6: Effect of adhesion (top) $\bar{\gamma}$ with $\bar{\sigma}=2$ and membrane tension (bottom) $\bar{\sigma}$ with $\bar{\gamma}=10$ on the wrapping, $f=0.8$. The r axis was truncated to $(-10;10)$. For the same value of f, the NP is fully wrapped by the cell only for $\bar{\sigma}=0.5$.

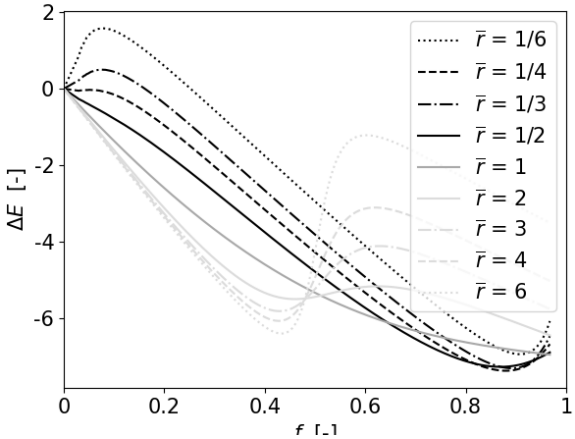

FIG. 7: $\Delta E(f)$ for the aspect ratios introduced in the table I. $\bar{\gamma}=10$, $\bar{\sigma}=2$.

Except for circular and slightly vertical particle ($\bar{r}\in[1/2,1]$), there is an energy barrier. The energy barrier takes place at low f for vertical ellipses and at f close to 0.5 for horizontal ellipses. It is easy for the horizontal ellipse to reach $f=0.5$, since it is basically the contact between the particle and the membrane, without even bending the latter. The vertical particle tends to stay as a very low f because it is necessary to bend a lot the cell membrane to increase f (see figure 8).

However, the energy barrier to overcome is lower for vertical than for horizontal particles. As illustrated in the figure 9, this barrier for vertical ellipses is reduced for lower $\bar{\sigma}$ and higher $\bar{\gamma}$, while the energy barrier for horizontal ellipses is only slightly reduced by lowering $\bar{\sigma}$.

To understand better on the influence of $\bar{r}$ and

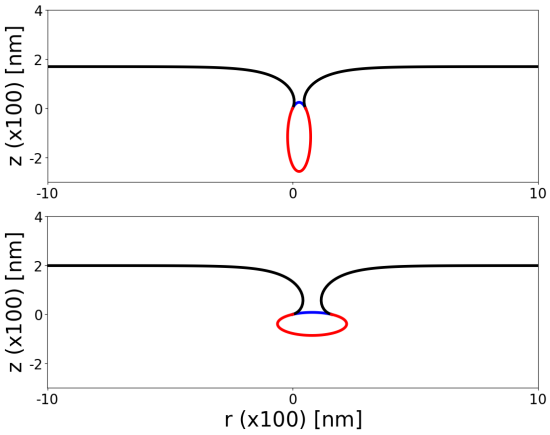

FIG. 8: Shape of contact region for vertical (top) and horizontal (bottom) ellipses with respective aspect ratio $\frac{1}{4}$ and 4, $\bar{\gamma} = 10$, $\bar{\sigma} = 2$, $f = 0.8$. Both ellipses' perimeter is 2π.

to generalize the results to a large range of $\bar{\gamma}$ and $\bar{\sigma}$, one can observe the phase diagram on the figure 10, where the proportion of the three phases is represented, for vertical and horizontal ellipses. The observations made previously are still valid in this graph. Indeed, the horizontal particles remain mainly in the phase 2 while the vertical ones remain in the phase 1. However, vertical particles tend to reach the phase 3 while horizontal particles usually do not overcome the phase 2. For excessively elongated particles neither the vertical nor the horizontal particles reach phase 3.

Probabilistic modeling of the random wrapping degree

Random input parameters

In this section the mechanical parameters of the nanoparticle $\bar{\gamma}$, $\bar{\sigma}$ along with its aspect ratio $r = a/b$ are modeled as random variables (denoted hereinafter by ($\bar{\Gamma}$,$\bar{\Sigma}$,R)). The objective is to first model these parameters via some appropriate probability distributions and then investigate the probabilistic content of the random wrapping degree $F = \Xi(\bar{\Gamma}, \bar{\Sigma}, R)$. Based on the literature (refs to be put here), we consider the following intervals for the aforementioned random variables: $\bar{\gamma} \in [1, 8]$, $\bar{\sigma} \in [0.5, 5.5]$ and $r \in [1, 8]$. Based on the maximum entropy principle (ref) since the only available information is the lower and upper bounds, the best candidate for the probability density function (PDF) (that maximizes the entropy measure) is the uniform distribution. However, a uniform distribution for the

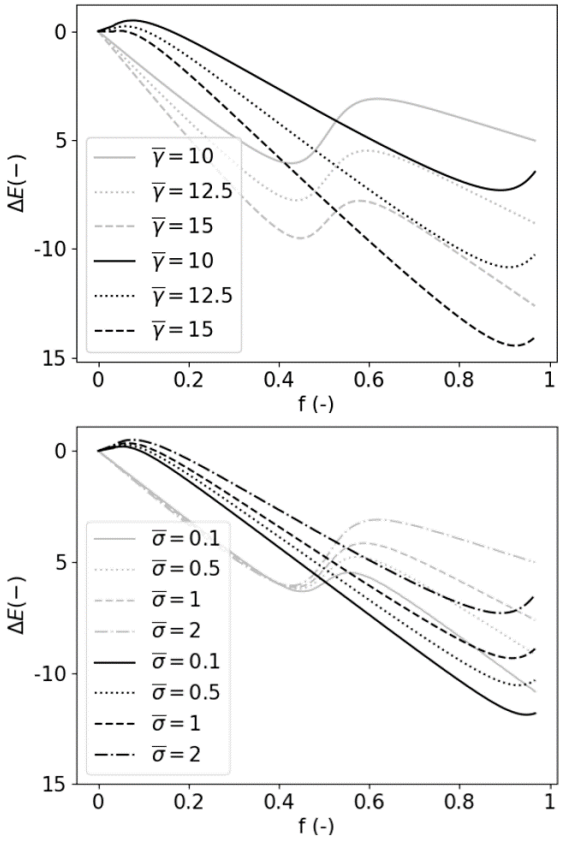

FIG. 9: Influence of (top) $\bar{\gamma}$ with $\bar{\sigma} = 2$ and (bottom) $\bar{\sigma}$ with $\bar{\gamma} = 10$ on $\Delta E(f)$ on elliptic particles. Dark line: vertical particle ($\bar{r} = 1/4$); Light line: horizontal particle ($\bar{r} = 4$).

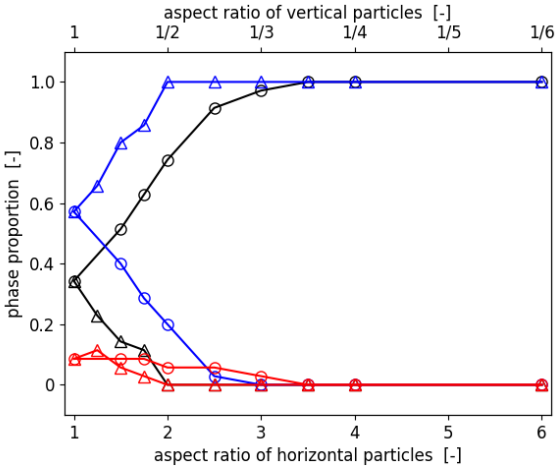

FIG. 10: Proportion of each phase depending on the aspect ratio of the particle. The triangles correspond to horizontal ellipses while the circles stand for vertical ones. The phases 1, 2 and 3 are respectively represented with black, blue and red line.

ratio R will result in samples that are biased towards more horizontal NPs since they will have 6 times more chance to be produced. To overcome this issue, we used a transformed beta distribution to model R, i.e. $R \sim \beta(0.5, 1.7; 1/6, 6)$. The particularity of this PDF is that its median is $r = 1$ so that $\mathsf{P}(R < 1) = \mathsf{P}(R > 1) = 0.5$ almost surely. As such, the input parameters as modeled as three independent random variables $\bar{\Gamma} \sim \mathcal{U}(1, 8)$, $\bar{\Sigma} \sim \mathcal{U}(0.5, 5.5)$ and $R \sim \beta(0.5, 1.7; 1/6, 6)$.

Sampling the random wrapping degree

Once the uncertainties related to each input parameter is characterized, a random sample of size 1000 based on quasi Monte Carlo (QMC) sampling method is generated. The corresponding values of the wrapping degree for each realization are then calculated. Figure 11 depicts the convergence of the average and coefficient of variation of the random wrapping degree in terms of the number of samples. It seems that a sample size of at least 800 should be used to guarantee the convergence of the first and second order statistics. This justifies the importance of using surrogate models allowing us to approximate the probabilistic content of the random wrapping degree using small sample sizes.

Surrogate modeling

In this section the PDF of the random wrapping degree F is modeled using two different surrogate modeling approaches.

The Kriging model is constructed based on the following parameters. For the trend part, a quadratic function as $\boldsymbol{a}^\top \boldsymbol{g}(\boldsymbol{x}) = a_0 + \sum_{i=1}^{M} a_i x_i + \sum_{i=1}^{M} \sum_{j=1}^{M} a_{ij} x_{ij}$ is used with coefficients to be determined. The ACF that is used to model the correlation function of the Gaussian process is von Kármán, i.e. $R(\eta, H) = 2(\sqrt{H}\eta)^H \mathcal{K}_H(2\sqrt{H}\eta)/\Gamma(H)$ wherein $\eta = h/\ell$, the shape parameter $H = 1.5$, Γ is the Gamma function and $\mathcal{K}_H$ is the modified Bessel function of the second kind. To solve the optimization problem (12) for the hyperparameter $\boldsymbol{\ell}$, a hybrid genetic algorithm [54] with upper and lower bounds of $[0.001, 10]$ for each ℓ_i $(1 \leq i \leq M)$ is used.

To build the PCE response surface, the polynomial degree p is chosen such that the corresponding LOO error is minimized. For this purpose, we varied p from 1 to 30 and calculated the error.

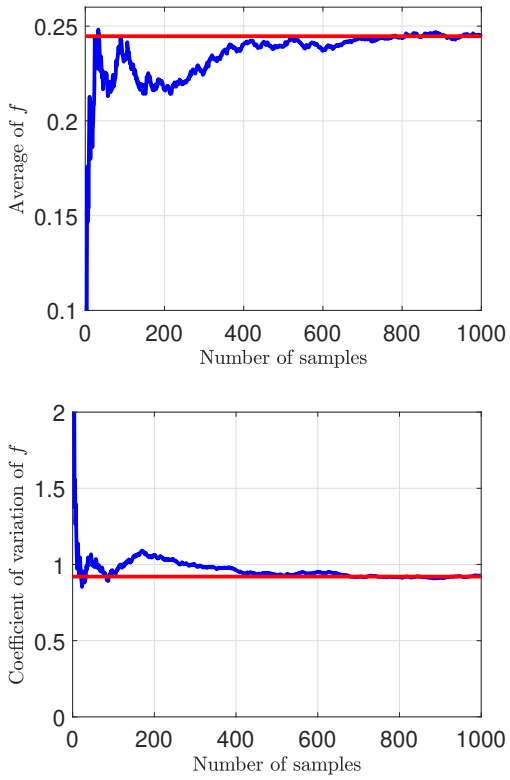

FIG. 11: Convergence of the first and second order statistics of the random wrapping degree for a QMC sample of size 1000. Blue and red curves correspond to the simulation data and the target value, respectively.

Figure 12 shows that $p = 22$ minimizes the error ($\epsilon_{LOO} = 0.045$) and will be used to construct the PCE model.

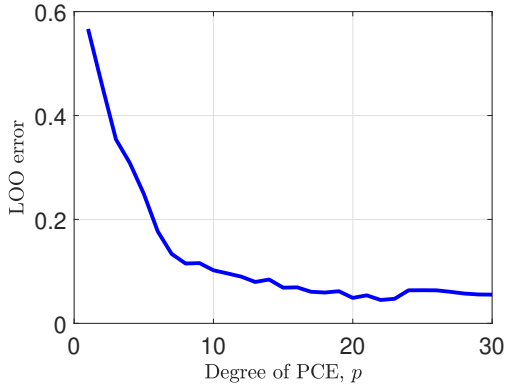

FIG. 12: Variation of the LOO error estimate in terms of the degree p of the PCE.

Theses response surfaces are now evaluated, with a near-zero computational cost, using a sample of size 10^5 and the estimated PDFs of F are compared

to the histogram of the simulated data in Figure 13. We can then estimate for instance the probability of *no wrapping* $\mathsf{P}(F < 0.2)$ (phase 1). The latter is 0.033, 0.032 and 0.036 based on the simulation data, Kriging and PCE, respectively, which shows the accuracy of the metamodels.

The Sobol' sensitivity indices are finally estimated using both metamodeling approaches. Kriging yields the following first-order indices ?,?,?. On the other hand, based on the PCE method, we get the values of 0.15, 0.07 and 0.46 (for $\bar{\Gamma}$, $\bar{\Gamma}$ and R, respectively) which reveals that if we consider the effect of the variability of each single input random variables on the variance of the random wrapping degree, the aspect ratio of the nanoparticle $r = a/b$ is the most influential. Then the adhesion $\bar{\gamma}$ contributes twice as large as the membrane tension $\bar{\sigma}$. The total sensitivity indices for $\bar{\Gamma}$, $\bar{\Gamma}$ and R are 0.4, 0.24 and 0.74, respectively. The difference $S_{T_i} - S_i$ shows the influence of the interactions on the variance of F. This difference is in the same order as for the first-order indices, i.e. the interactions of R with other inputs contributes the most on the variability of the wrapping degree.

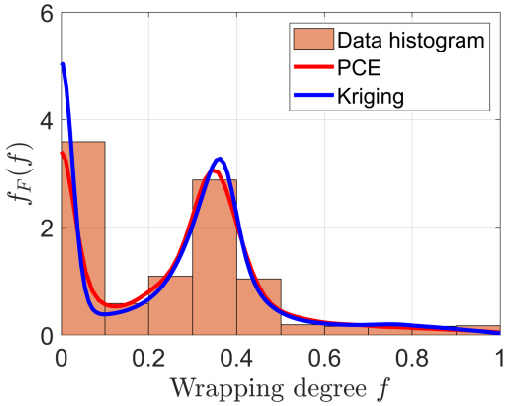

FIG. 13: Estimations of the PDF of the random wrapping degree obtained by Kriging and PCE metamodels.

DISCUSSION

Cell membrane reorganization during endocytosis

This paper only considers constant values of $\bar{\sigma}$ and $\bar{\gamma}$ during endocytosis, while they are actually variable with respect to f, as explained in [18, 22, 55–61]. Indeed, the cell tends to adapt to the phenomenon by simultaneously increasing the amount of interaction at the contact region (and consequently increasing the adhesion) and reorganizing its actin network, helping to the membrane deformation (and consequently increasing the tension). It may explain why the observations conducted *in vivo* [7, 8] concluded that vertical elliptic nanoparticles had higher chances to enter the cell than horizontal ones in almost all cases. Indeed, the variation of the mechanical properties leads to vanish the energy barrier.

Rotation of elliptic NP during endocytosis

It was also found experimentally [62] and numerically [12, 63, 64] that if an elliptic particle touches the membrane by its horizontal side, it will tend to rotate to be engulfed vertically. However, it appears to depend on the membrane tension, as demonstrated in [9] : the NP is wrapped in its vertical configuration if the tension is inferior to a threshold $\bar{\sigma}$ and in its horizontal configuration otherwise.

Heterogeneity and composition of the cell membrane

In this study, the NP was considered as about 10 times smaller than the cell and the system was set at the NP's scale (about 100 nm). However, membrane's thickness is around 4 nm, and is composed of several trans-membrane proteins, whose length can reach 16 nm [65]. Consequently, they could play a role in this interaction and directly interact with the particle.

Moreover, the membrane is highly heterogeneous and composed of various components (mainly carbohydrates, proteins and lipids) [31, 66]. The outer part of the membrane is also covered by a sugar layer, called *glycocalyx* or *fuzzy coat* [67, 68], which alters with the interaction with the extra-cellular middle by reducing the adhesion. The presence of glycocalyx is usually more important in cancer cells than in healthy cells [17], meaning that it is a parameter to take into account to model the adhesion between the cell and the NP.

Moreover, the cell membrane is not homogeneous alongside the perimeter of the cell. For instance, there are lipid rafts [32, 69], which are parts of the membrane more rigid than the rest of the membrane.

The former facts about the structure of the cell membrane call the hypothesis of a smooth and homogeneous region 3 into question.

However, since the study was performed for a range of $\bar{\gamma}$ and $\bar{\sigma}$, our results still apply by accounting

for the variability of the membrane's properties.

Rigidity of the NP

Our model was built considering a rigid NP. As explained in the hypothesis section, this choice was made for the sake of simplification and it appeared to fit with many of the existing NP. However, NP with low bending rigidity (in the same order of magnitude as the membrane) exist as well [14]. Moreover, previous studies [12, 15] demonstrated that the rigidity of the NP is a prominent parameter of endocytosis. Consequently, additional investigations should be performed accounting for the rigidity of the NP to provide results adapted to a larger range of NP.

Full wrapping and endocytosis

The wrapping of the NP is actually the very first step of endocytosis [70]. Indeed, it is not sure that the NP will not be ejected (via *exocytosis*) before reaching its target [32].

2D model

Zhou *et. al* [24] suppose that 2D model suits for the study of the adhesion of a vesicle to a substrate. However, Yi *et. al* [15] performed both 2D and 3D axisymmetric models of the cellular uptake of a NP and found the same results for circular NPs but different behavior of $\Delta E(f)$ for other shapes. Indeed, for non-circular particles, studying only one section of the NP is not enough to have a full picture of the wrapping since it would not account for all the bending of the membrane.

CONCLUSION

This work presented a 2D model of the cellular uptake of a rigid elliptic NP at the scale of the NP. Based on the latter, investigations have been conducted to evaluate the influence of the mechanical properties of the cell membrane coupled with the aspect ratio of the elliptic rigid particle on the cellular uptake of NP. Afterwards, a sensitivity analysis of these results highlighted that they are twice more sensitive to the NP's aspect ratio than to the adhesion, which influences twice more than the membrane tension.

As suggestions for future research, the influence of the deformability of the particle and the variation of the mechanical properties of the cell during wrapping should be investigated.

SUPPLEMENTAL MATERIAL

The Python code used to display the wrapping, compute $\Delta E(f)$ and to identify the wrapping phases is available at the following address : `https://uncloud.univ-nantes.fr/index.php/s/PqBJkZ66YSAHeGk`

ACKNOWLEDGMENTS

This work was supported by ...

* sarah.iaquinta@univ-nantes.fr

[1] Jörg Kreuter. Nanoparticles—a historical perspective. *International journal of pharmaceutics*, 331(1):1–10, 2007.

[2] Mark E Davis, Zhuo Chen, and Dong M Shin. Nanoparticle therapeutics: an emerging treatment modality for cancer. *Nanoscience and technology: A collection of reviews from nature journals*, pages 239–250, 2010.

[3] Xinghua Shi, Annette von Dem Bussche, Robert H Hurt, Agnes B Kane, and Huajian Gao. Cell entry of one-dimensional nanomaterials occurs by tip recognition and rotation. *Nature nanotechnology*, 6(11):714–719, 2011.

[4] B Devika Chithrani, Arezou A Ghazani, and Warren CW Chan. Determining the size and shape dependence of gold nanoparticle uptake into mammalian cells. *Nano letters*, 6(4):662–668, 2006.

[5] Laura Florez, Christine Herrmann, Jens M Cramer, Christoph P Hauser, Kaloian Koynov, Katharina Landfester, Daniel Crespy, and Volker Mailänder. How shape influences uptake: interactions of anisotropic polymer nanoparticles and human mesenchymal stem cells. *Small*, 8(14):2222–2230, 2012.

[6] Jin-Wook Yoo and Samir Mitragotri. Polymer particles that switch shape in response to a stimulus. *Proceedings of the National Academy of Sciences*, 107(25):11205–11210, 2010.

[7] Julie A Champion, Yogesh K Katare, and Samir Mitragotri. Making polymeric micro-and nanoparticles of complex shapes. *Proceedings of the National Academy of Sciences*, 104(29):11901–11904, 2007.

[8] Julie A Champion and Samir Mitragotri. Role of target geometry in phagocytosis. *Proceedings of the National Academy of Sciences*, 103(13):4930–4934, 2006.

[9] Xin Yi, Xinghua Shi, and Huajian Gao. A universal law for cell uptake of one-dimensional nanomaterials. *Nano letters*, 14(2):1049–1055, 2014.

[10] Sovan Das and Qiang Du. Adhesion of vesicles to curved substrates. *Physical Review E*, 77(1):011907, 2008.

[11] Amir Houshang Bahrami. Orientational changes and impaired internalization of ellipsoidal nanoparticles by vesicle membranes. *Soft Matter*, 9(36):8642–8646, 2013.

[12] Xin Yi and Huajian Gao. Phase diagrams and morphological evolution in wrapping of rod-shaped elastic nanoparticles by cell membrane: a two-dimensional study. *Physical Review E*, 89(6):062712, 2014.

[13] Robert Vácha, Francisco J Martinez-Veracoechea, and Daan Frenkel. Receptor-mediated endocytosis of nanoparticles of various shapes. *Nano letters*, 11(12):5391–5395, 2011.

[14] Changjin Huang, Yao Zhang, Hongyan Yuan, Huajian Gao, and Sulin Zhang. Role of nanoparticle geometry in endocytosis: laying down to stand up. *Nano letters*, 13(9):4546–4550, 2013.

[15] Xin Yi, Xinghua Shi, and Huajian Gao. Cellular uptake of elastic nanoparticles. *Physical review letters*, 107(9):098101, 2011.

[16] Sulin Zhang, Huajian Gao, and Gang Bao. Physical principles of nanoparticle cellular endocytosis. *ACS nano*, 9(9):8655–8671, 2015.

[17] M Abercrombie and EJ Ambrose. The surface properties of cancer cells: a review. *Cancer research*, 22(5 Part 1):525–548, 1962.

[18] LB Freund and Yuan Lin. The role of binder mobility in spontaneous adhesive contact and implications for cell adhesion. *Journal of the Mechanics and Physics of Solids*, 52(11):2455–2472, 2004.

[19] Christine Vauthier and Kawthar Bouchemal. Methods for the preparation and manufacture of polymeric nanoparticles. *Pharmaceutical research*, 26(5):1025–1058, 2009.

[20] Wolfgang Helfrich. Elastic properties of lipid bilayers: theory and possible experiments. *Zeitschrift für Naturforschung c*, 28(11-12):693–703, 1973.

[21] Hervé Hillaireau and Patrick Couvreur. Nanocarriers' entry into the cell: relevance to drug delivery. *Cellular and molecular life sciences*, 66(17):2873–2896, 2009.

[22] Gang Bao and Subra Suresh. Cell and molecular mechanics of biological materials. *Nature materials*, 2(11):715–725, 2003.

[23] Stephen Cooper. Control and maintenance of mammalian cell size. *BMC cell biology*, 5(1):1–21, 2004.

[24] Xiao-Hua Zhou, Jian-Lin Liu, and Sheng-Li Zhang. Adhesion of a vesicle on an elastic substrate: 2d analysis. *Colloids and Surfaces B: Biointerfaces*, 110:372–378, 2013.

[25] Martin Michael Müller, Markus Deserno, and Jemal Guven. Balancing torques in membrane-mediated interactions: exact results and numerical illustrations. *Physical Review E*, 76(1):011921, 2007.

[26] Markus Deserno and Thomas Bickel. Wrapping of a spherical colloid by a fluid membrane. *EPL (Europhysics Letters)*, 62(5):767, 2003.

[27] Christian Dietrich, Miglena Angelova, and Bernard Pouligny. Adhesion of latex spheres to giant phospholipid vesicles: statics and dynamics. *Journal de Physique II*, 7(11):1651–1682, 1997.

[28] Christian Dietrich, Miglena Angelova, and Bernard Pouligny. Adhesion of latex spheres to giant phospholipid vesicles: statics and dynamics. *Journal de Physique II*, 7(11):1651–1682, 1997.

[29] Huajian Gao, Wendong Shi, and Lambert B Freund. Mechanics of receptor-mediated endocytosis. *Proceedings of the National Academy of Sciences*, 102(27):9469–9474, 2005.

[30] Markus Deserno. Elastic deformation of a fluid membrane upon colloid binding. *Physical Review E*, 69(3):031903, 2004.

[31] S Jonathan Singer and Garth L Nicolson. The fluid mosaic model of the structure of cell membranes. *Science*, 175(4023):720–731, 1972.

[32] Gary J Doherty and Harvey T McMahon. Mechanisms of endocytosis. *Annual review of biochemistry*, 78:857–902, 2009.

[33] Mark B Villarino. Ramanujan's perimeter of an ellipse. *arXiv preprint math/0506384*, 2005.

[34] J. Sacks, W. J. Welch, T. J. Mitchell, and H. P. Wynn. Design and analysis of computer experiments. *Statistical science*, pages 409–423, 1989.

[35] M. L. Stein. *Interpolation of spatial data: some theory for kriging*. Springer Science & Business Media, 2012.

[36] T. J. Santner, B. J. Williams, and W. I. Notz. *The design and analysis of computer experiments*. Springer Science & Business Media, 2013.

[37] C. E. Rasmussen. Gaussian processes in machine learning. In *Advanced lectures on machine learning*, pages 63–71. Springer, 2004.

[38] Roger G Ghanem and Pol D Spanos. *Stochastic finite elements: a spectral approach*. Dover publications, 2003.

[39] S.-K. Choi, R. V. Grandhi, R. A. Canfield, and C. L. Pettit. Polynomial chaos expansion with Llatin hypercube sampling for estimating response variability. *American Institute of Aeronautics and Astronautics*, 42(6):1191–1198, 2004.

[40] M. Berveiller, B. Sudret, and M. Lemaire. Stochastic finite element: a non intrusive approach by regression. *European Journal of Computational Mechanics/Revue Européenne de Mécanique Numérique*, 15(1-3):81–92, 2006.

[41] B. Sudret. Global sensitivity analysis using polynomial chaos expansions. *Reliability Engineering & System Safety*, 93(7):964–979, 2008.

[42] A. Marrel, B. Iooss, F. Van Dorpe, and E. Volkova. An efficient methodology for modeling complex computer codes with Gaussian processes. *Computational Statistics & Data Analysis*, 52(10):4731–4744, 2008.

[43] V. Dubourg, B. Sudret, and J. M. Bourinet. Reliability-based design optimization using kriging surrogates and subset simulation. *Structural*

and Multidisciplinary Optimization, 44(5):673–690, 2011.

[44] C. Lataniotis, S. Marelli, and B. Sudret. Gaussian process modelling using UQLab. *arXiv preprint arXiv:1709.09382*, 2017.

[45] G. Blatman and B. Sudret. An adaptive algorithm to build up sparse polynomial chaos expansions for stochastic finite element analysis. *Probabilistic Engineering Mechanics*, 25(2):183–197, 2010.

[46] O. Dubrule. Cross validation of kriging in a unique neighborhood. *Journal of the International Association for Mathematical Geology*, 15(6):687–699, 1983.

[47] R. G. Ghanem and P. D. Spanos. Stochastic finite element method: Response statistics. In *Stochastic finite elements: a spectral approach*, pages 101–119. Springer, 1991.

[48] O. Le Maître and O. M. Knio. *Spectral methods for uncertainty quantification: with applications to computational fluid dynamics*. Springer Science & Business Media, 2010.

[49] E. Savin and B. Faverjon. Computation of higher-order moments of generalized polynomial chaos expansions. *International Journal for Numerical Methods in Engineering*, 111(12):1192–1200, 2017.

[50] I. Sobol. Sensitivity estimates for non-linear mathematical models. *Mathematical Modeling and Computational Experiment*, 1(4):407–414, 1993.

[51] A. Saltelli, P. Annoni, I. Azzini, F. Campolongo, M. Ratto, and S. Tarantola. Variance-based sensitivity analysis of model output. Design and estimator for the total sensitivity index. *Computer Physics Communications*, 181(2):259–270, 2010.

[52] T. Homma and A. Saltelli. Importance measures in global sensitivity analysis of nonlinear models. *Reliability Engineering & System Safety*, 52(1):1–17, 1996.

[53] Arnaud Vonarbourg, Catherine Passirani, Patrick Saulnier, and Jean-Pierre Benoit. Parameters influencing the stealthiness of colloidal drug delivery systems. *Biomaterials*, 27(24):4356–4373, 2006.

[54] T. A. El-Mihoub, A. A. Hopgood, L. Nolle, and A. Battersby. Hybrid genetic algorithms: A review. *Engineering Letters*, 13(2):124–137, 2006.

[55] Margarita Staykova, Marino Arroyo, Mohammad Rahimi, and Howard A Stone. Confined bilayers passively regulate shape and stress. *Physical review letters*, 110(2):028101, 2013.

[56] Xin Yi and Huajian Gao. Kinetics of receptor-mediated endocytosis of elastic nanoparticles. *Nanoscale*, 9(1):454–463, 2017.

[57] Hongyan Yuan, Ju Li, Gang Bao, and Sulin Zhang. Variable nanoparticle-cell adhesion strength regulates cellular uptake. *Physical review letters*, 105(13):138101, 2010.

[58] Hiroshi Noguchi and Masako Takasu. Adhesion of nanoparticles to vesicles: a brownian dynamics simulation. *Biophysical journal*, 83(1):299–308, 2002.

[59] Andre E Nel, Lutz Mädler, Darrell Velegol, Tian Xia, Eric MV Hoek, Ponisseril Somasundaran, Fred Klaessig, Vince Castranova, and Mike Thompson. Understanding biophysicochemical interactions at the nano–bio interface. *Nature materials*, 8(7):543–557, 2009.

[60] Anita Joanna Kosmalska, Laura Casares, Alberto Elosegui-Artola, Joseph Jose Thottacherry, Roberto Moreno-Vicente, Víctor González-Tarragó, Miguel Ángel Del Pozo, Satyajit Mayor, Marino Arroyo, Daniel Navajas, et al. Physical principles of membrane remodelling during cell mechanoadaptation. *Nature communications*, 6(1):1–11, 2015.

[61] P Decuzzi and Mauro Ferrari. The receptor-mediated endocytosis of nonspherical particles. *Biophysical journal*, 94(10):3790–3797, 2008.

[62] Xinghua Shi, Annette von Dem Bussche, Robert H Hurt, Agnes B Kane, and Huajian Gao. Cell entry of one-dimensional nanomaterials occurs by tip recognition and rotation. *Nature nanotechnology*, 6(11):714–719, 2011.

[63] Amir Houshang Bahrami. Orientational changes and impaired internalization of ellipsoidal nanoparticles by vesicle membranes. *Soft Matter*, 9(36):8642–8646, 2013.

[64] Sabyasachi Dasgupta, Thorsten Auth, and Gerhard Gompper. Shape and orientation matter for the cellular uptake of nonspherical particles. *Nano letters*, 14(2):687–693, 2014.

[65] Weidong Zhao, Yongmei Tian, Mingjun Cai, Feng Wang, Jiazhen Wu, Jing Gao, Shuheng Liu, Junguang Jiang, Shibo Jiang, and Hongda Wang. Studying the nucleated mammalian cell membrane by single molecule approaches. *PLoS One*, 9(5):e91595, 2014.

[66] Garth L Nicolson. Update of the 1972 singer-nicolson fluid-mosaic model of membrane structure. *Discoveries*, 1(1), 2013.

[67] Cuixia Yang, Yiwen Liu, Yiqing He, Yan Du, Wenjuan Wang, Xiaoxing Shi, and Feng Gao. The use of ha oligosaccharide-loaded nanoparticles to breach the endogenous hyaluronan glycocalyx for breast cancer therapy. *Biomaterials*, 34(28):6829–6838, 2013.

[68] Susumu Ito. The enteric surface coat on cat intestinal microvilli. *The Journal of cell biology*, 27(3):475–491, 1965.

[69] John A Allen, Robyn A Halverson-Tamboli, and Mark M Rasenick. Lipid raft microdomains and neurotransmitter signalling. *Nature reviews neuroscience*, 8(2):128–140, 2007.

[70] Shahed Behzadi, Vahid Serpooshan, Wei Tao, Majd A Hamaly, Mahmoud Y Alkawareek, Erik C Dreaden, Dennis Brown, Alaaldin M Alkilany, Omid C Farokhzad, and Morteza Mahmoudi. Cellular uptake of nanoparticles: journey inside the cell. *Chemical Society Reviews*, 46(14):4218–4244, 2017.